Since January 2020 Elsevier has created a COVID-19 resource centre with free information in English and Mandarin on the novel coronavirus COVID-19. The COVID-19 resource centre is hosted on Elsevier Connect, the company's public news and information website.

European Journal of Radiology 134 (2021) 109442

Contents lists available at ScienceDirect

European Journal of Radiology

journal homepage: www.elsevier.com/locate/ejrad

Research article

CT features of coronavirus disease 2019 (COVID-19) with an emphasis on the vascular enlargement pattern

Qi Li [a,1], Xing-Tao Huang [b,1], Chun-Hua Li [c], Dan Liu [d], Fa-Jin Lv [a,*]

[a] Department of Radiology, The First Affiliated Hospital of Chongqing Medical University, No.1 Youyi Road, Yuzhong District, Chongqing, 400016, China
[b] Department of Radiology, University of Chinese Academy of Sciences Chongqing Renji Hospital (Fifth People's Hospital of Chongqing), No. 24 Renji Road, Nan'an District, Chongqing, China
[c] Department of Radiology, Chongqing Public Health Medical Center, No. 109 Baoyu Road, Shapingba District, Chongqing, 400036, China
[d] Department of Radiology, Yongchuan Hospital of Chongqing Medical University, No. 439 Xuanhua Road, Yongchuan District, Chongqing, 402160, China

ARTICLE INFO

Keywords:
Coronavirus disease 2019
Pneumonia
Tomography
X-Ray computed

ABSTRACT

Purpose: The vascular enlargement (VE) pattern differs from previously described imaging patterns for pneumonia. This study aimed to investigate the incidence, computed tomography (CT) characteristics, and diagnostic value of the VE pattern in coronavirus disease 2019 (COVID-19).

Method: The CT data of 106 patients with COVID-19 from January 19 to February 29, 2020, and 52 patients with influenza virus pneumonia (IVP) from January 2018 to February 2020 were retrospectively collected. The incidences of the VE pattern between the two groups were compared. The CT manifestations of COVID-19 were analyzed with a particular focus on the VE pattern's specific CT signs, dynamic changes, and relationships with lesion size and disease severity.

Results: Peripheral and multilobar ground-glass opacities (GGOs) or mixed GGOs with various sizes and morphologies were typical features of COVID-19 on initial CT. The VE pattern was more common in COVID-19 (88/106, 83.02 %) than in IVP (10/52, 19.23 %) on initial CT ($P < 0.001$). Three special VE-pattern-specific CT signs, including central vascular sign, ginkgo leaf sign, and comb sign, were identified. Four types of dynamic changes in the VE pattern were observed on initial and follow-up CT, which were closely associated with the evolution of lesions and the time interval from the onset of symptoms to initial CT scan. The VE pattern in COVID-19 was more commonly seen in larger lesions and patients with severe–critical type (all $P < 0.001$).

Conclusions: The VE pattern is a valuable CT sign for differentiating COVID-19 from IVP, which correlates with more extensive or serious disease. A good understanding of the CT characteristics of the VE pattern may contribute to the early and accurate diagnosis of COVID-19 and prediction of the evolution of lesions.

1. Introduction

A novel coronavirus, severe acute respiratory syndrome coronavirus 2 (SARS-CoV-2) that causes coronavirus disease 2019 (COVID-19), is responsible for the current 2020 major pandemic. COVID-19 is highly infectious in humans [1]. As of April 2, 2020, the World Health Organization has reported >1 million confirmed cases and >50,000 deaths related to COVID-19 worldwide. In the absence of effective therapies or specific COVID-19 vaccines, early recognition and timely isolation of infected persons is necessary to control this outbreak.

The standard diagnostic method for COVID-19 is real-time polymerase chain reaction (RT-PCR) to detect the SARS-CoV-2 nucleic acid in respiratory secretion specimens obtained by oropharyngeal or nasopharyngeal swab, bronchoalveolar lavage, or tracheal aspirate [2, 3]. However, recently, it has been revealed that RT-PCR results often lack high sensitivity and sufficient stability, which might be attributed to low virus titers within samples or technical issues, and require a relatively long processing time [4–7]. By contrast, chest computed tomography (CT) has high sensitivity and can obtain results rapidly [4–7]. A recent study by Ai et al. [6] reported that 59 % patients with COVID-19 had positive RT-PCR results and 88 % had positive chest CT scans; additionally, chest CT had 97 % sensitivity in predicting COVID-19.

* Corresponding author.
E-mail addresses: zhuoshui@sina.com (Q. Li), 80209749@qq.com (X.-T. Huang), 1683290633@qq.com (C.-H. Li), 5677676@qq.com (D. Liu), lvfj2020@sina.com (F.-J. Lv).
[1] Qi Li and Xing-Tao Huang contributed equally to this work.

https://doi.org/10.1016/j.ejrad.2020.109442
Received 6 May 2020; Received in revised form 22 November 2020; Accepted 25 November 2020
Available online 27 November 2020

Similarly, Long et al. [7] found that the chest CT sensitivity for COVID-19 infection was 97.2 % compared with the RT-PCR sensitivity of 71 %. Therefore, some investigators think that CT can be used as an important complement to RT-PCR, particularly for patients with COVID-19 with false negative RT-PCR results [4–8]. According to recent reports, most patients with COVID-19 share typical CT appearances, including bilateral ground-glass opacities (GGOs), multifocal patchy consolidation, and interstitial thickening with a subpleural distribution [9–12]. However, these imaging features were thought to be nonspecific because they were also frequently observed in patients with other types of pneumonia [12,13].

In clinical practice, we have found that vascular enlargement (VE) pattern presents in most of our patients with COVID-19, which is characterized by dilatation of pulmonary vessels around and within the lesions on CT images. This particular CT feature is different from the previous imaging descriptions for pneumonia, which led us to wonder if the CT characteristics are specific to COVID-19. However, the related radiologic characteristics and diagnostic value of the VE pattern in COVID-19 have not yet been investigated in detail. Herein, we aimed to investigate the incidence, CT characteristics, and diagnostic value of the VE pattern in COVID-19.

2. Materials and methods

2.1. Patients

This study was approved by the ethics committee of our institution, and informed consent was waived. From January 19 to February 29, 2020, 125 patients with a diagnosis of COVID-19 confirmed by nucleic acid testing in three institutions in China, who did not have severe cardiopulmonary diseases (e.g. pulmonary hypertension, heart failure) which might contribute to VE, underwent serial chest CT examinations. Among these patients, 19 with negative chest CT were excluded. In total, 106 patients were included. We also retrospectively collected the initial CT data of 52 patients with laboratory-confirmed influenza virus pneumonia (IVP) who had been admitted in our hospital between January 2018 and February 2020, including 47 patients with influenza A virus pneumonia and five patients with influenza B virus pneumonia.

2.2. CT protocols

All chest CT examinations were performed using the following three scanners: Discovery CT750HD (GE Healthcare), Toshiba Aquilion 16 (Toshiba Medical Systems), and Brilliance iCT (Philips Healthcare). All patients underwent noncontrast-enhanced scanning in the supine position. The imaging parameters were as follows: tube voltage, 100–130 kV; tube current, 100–400 mA; and scanning slice thickness, 5 mm. All images were reconstructed using 1-mm or 1.25-mm thin slices and stored on an ADW 4.6 workstation (GE Healthcare). Generally, follow-up CT scans were performed every 5–7 days for assessing disease progression after a short-term regular treatment. When the patient's symptoms worsened or the treatment protocols changed, the follow-up interval was shortened according to the patient's condition. Finally, the follow-up interval for our patients was 3–7 days. Among them, 61 patients had undergone four follow-up CT scans, 18 patients had undergone five follow-up CT scans, and 27 patients had undergone six follow-up CT scans.

Table 1
Clinical characteristics of study population.

Characteristics	COVID-19 (n = 106)	IVP (n = 52)
Sex		
Men	50 (47.17 %)	24 (46.15 %)
Women	56 (52.83 %)	28 (53.85 %)
Age (years)		
Mean ± standard deviation	50 ± 15	42 ± 11
Range	10–81	15–62
Comorbidities		
Patients with cardiovascular disease	16 (15.09 %)	12 (23.08 %)
Patients with hypertension	21 (19.81 %)	15 (28.85 %)
Patients with diabetes	12 (11.32 %)	6 (11.54 %)
Time interval from the onset of symptoms to initial CT (days)		
Median ± interquartile range	6.50 ± 8	5.50 ± 5
Range	1−18	1−16
Patient outcome		
Cured patients	106 (100 %)	52 (100 %)
Dead patients	0 (0 %)	0 (0 %)

COVID-19, coronavirus disease 2019; IVP, influenza virus pneumonia; CT, computed tomography.

2.3. CT image analysis

Two experienced radiologists with >10 years of experience in chest imaging who were blinded to the related clinical data interpreted the axial images with 5-mm slice thickness on the workstations, assisted by thin-slice images and 10-mm maximum-intensity projection images. Any disagreement was resolved by discussion to reach a consensus. For each patient with COVID-19, the following data were carefully observed and recorded: (1) lobar involvement (multiple lobes/single lobe) and number of lesions for each patient on initial CT; (2) distribution (peripheral/central/both central and peripheral), location (left upper and lower lobes; right upper, middle, and lower lobes), density [GGO/mixed GGO (GGO admixed with consolidation)/consolidation], size (longest diameter of lesions on axial images in the lung window setting: window width, 1600 HU; window level, −600 HU), and shape [round-like, arch-shaped, fan-shaped, and patchy (triangular, rectangular, or trapezoidal)] of each lesion on initial CT; (3) presence of the VE pattern for each lesion on initial CT; (4) special CT signs related to the VE pattern; (5) dynamic changes in the VE pattern, and (6) developmental changes in lesions on initial and follow-up CT. In addition, for patients with IVP, presence of the VE pattern and common CT features on initial CT were analyzed. The criteria for assessing the presence of the VE pattern was as follows: 1) increased vascular diameter by comparing with that of other vessels of the same grade in the identical or other lung lobes; 2) increased vascular diameter relative to that of the same vessel on previous or later CT images. Lesions meeting any one of the above-mentioned criteria were considered to have the VE pattern. Furthermore, the VE pattern was only evaluated within areas of GGO or mixed GGO (hereinafter referred to as GGOs), and consolidated lesions were excluded from analysis because vessels within the lesions were obscured.

2.4. Clinical classifications for disease severity

Disease severity was classified into four categories according to the Guidelines for the Diagnosis and Treatment of COVID-19 issued by the National Health Commission (fifth edition; China) [14]: 1) mild type: mild clinical symptoms without pneumonia on CT imaging; 2) common type: fever and other symptoms of respiratory infection with pneumonia on CT imaging; 3) severe type: had a. respiratory distress with respiratory rate ≥ 30/min, b. oxygen saturation ≤ 93 % in the resting condition, and/or c. arterial partial pressure of oxygen/oxygen concentration ≤ 300 mmHg (1 mmHg = 0.133 kPa); 4) critical type: had a. respiratory failure requiring mechanical ventilation, b. shock, and/or c. required intensive care unit monitoring and treatment because of other organ failure.

2.5. Statistical analysis

Statistical analyses were performed using IBM SPSS Statistics for Windows (version 19,0; IBM Corp., Armonk, NY). Single-sample Kolmogorov–Smirnov analysis was used to test the variance in homogeneity of the measurements. Normally distributed quantitative data were

Table 2
General imaging findings of coronavirus disease 2019.

Characteristic	COVID-19 (number of lesions = 552)
Distribution	
Peripheral	398 (72.10 %)
Central	106 (19.20 %)
Both central and peripheral	48 (8.70 %)
Location	
Right upper lobe	126 (22.83 %)
Right middle lobe	58 (10.51 %)
Right lower lobe	135 (24.46 %)
Left upper lobe	109 (19.75 %)
Left lower lobe	124 (22.46 %)
Density	
GGO	350 (63.41 %)
Mixed GGO	180 (32.61 %)
Consolidation	22 (3.99 %)
Lesion sizes	
<3 cm	290 (52.54 %)
3–5 cm	111 (20.11 %)
>5 cm	151 (27.36 %)
Shape	
Round-like	270 (48.91 %)
Patchy	147 (26.63 %)
Arch-shaped	74 (13.41 %)
Fan-shaped	61 (11.05 %)

COVID-19, coronavirus disease 2019; GGO, ground-glass opacity.

expressed as means ± standard deviations, whereas nonnormally distributed data were presented as medians ± interquartile ranges. The two independent-samples Student's *t*-test was performed to assess parameters consistent with normal distribution; otherwise, the Mann–Whitney *U* test was performed. The frequencies of the VE pattern between COVID-19 and IVP, between different-sized lesions in COVID-19, and between patients with COVID-19 under different clinical classifications were compared using the chi-squared test. A two-tailed $P < 0.05$ indicated statistical significance.

3. Results

3.1. Clinical characteristics of study population

Clinical characteristics including sex, age, comorbidities, days from illness onset to initial CT, and outcome of the 106 patients with COVID-19 and the 52 patients with IVP are summarized in Table 1.

3.2. General imaging findings of COVID-19 on initial CT

Among the 106 patients with COVID-19, 82 (77.36 %) showed multilobar involvement, seven (6.60 %) showed single-lobar involvement with ≥2 lesions, and 17(16.04 %) showed single-lobar involvement with only one lesion. In total, 552 lesions were detected on initial CT. General CT findings of lesions including distribution, location, density, and lesion size and shape are shown in Table 2. Peripheral GGOs, mainly in the lower or upper lobes and less frequently within the right middle lobe, with various sizes and morphologies were the typical features of COVID-19 on initial CT.

3.3. Comparison of frequencies of the VE pattern between COVID-19 and IVP and common CT features of IVP on initial CT

Out of 106 patients with COVID-19, 88 (83.02 %) had the VE pattern on initial CT. Out of 52 patients with IVP, 10 (19.23 %) had the VE pattern. The chi-squared test showed that there was a significant difference between the VE pattern frequencies with COVID-19 and with IVP, indicating that the VE pattern was more common in patients with COVID-19 ($P < 0.001$). Among the 52 patients with IVP, 42 (80.77 %) showed multilobar involvement and 10 (19.23 %) showed single-lobar involvement. GGOs (94.23 %, 49/52) and consolidation (53.85 %, 28/52) with a predominant peribronchovascular and subpleural distribution were the most frequent CT signs, followed by the interstitial thickening (38.46 %, 20/52).

3.4. Special CT signs related to the VE pattern in COVID-19 on initial CT

A total of 530 lesions presented as GGOs on initial CT. Among them, 370 (69.81 %) lesions had the VE pattern. Three special CT signs related to the VE pattern based on the lesions' morphology were observed: 1) central vascular sign: characterized by ≥1 dilated vessels extending into or passing through the center of a round-like lesion, similar to a target, string bead, or hanging fruit according to the positional relationship between the lesions and vessels on axial CT images (96/370, 25.95 %) (Fig. 1); 2) ginkgo leaf sign: characterized by ≥1 trunks of dilated vessels extending into a fan-shaped lesion from its tip facing the hilar, resembling a ginkgo leaf (41/370, 11.08 %) (Fig. 2); 3) comb sign: characterized by multiple nearly parallel and dilated vessels vertically entering into a subpleural arch-shaped lesion, similar to a comb (51/370, 13.78 %) (Fig. 3).

3.5. Dynamic changes of the VE pattern in COVID-19 on initial and follow-up CT

As shown in Table 3, among 530 lesions with GGOs, four types of dynamic changes in the VE pattern were identified on serial CT, which correlated closely with the evolution of lesions: 1) type I (130/530, 24.53 %): the VE pattern was absent on both initial and follow-up CT. For this type, most lesions (115/130, 88.46 %) improved with an absorption of GGOs and sometimes appearance of fibrosis, whereas a small number of lesions (15/130, 11.54 %) progressed with an increase of GGOs or consolidation; 2) type II (30/530, 5.66 %): the VE pattern was absent on initial CT but present on follow-up CT. In the early stage, as the vessels dilated, the lesions advanced. Then, the lesions absorbed in different degrees as the vessels gradually became thin or remained unchanged (Figs. 3); 3) type III (236/530, 44.53 %): the VE pattern was present on initial CT, and then, the vessels gradually became thin or remained unchanged on follow-up CT. For this type, some lesions improved (90/236, 38.14 %), whereas others progressed (146/236, 61.86 %) (Fig. 2); 4) type IV (134/236, 25.28 %): the VE pattern was present on initial CT, and follow-up CT showed further enlargement of vessels with lesion progression, and then, the vessels gradually became thin or remained unchanged with lesion resolution in different degrees (Fig. 1).

Additionally, the dynamic changes of the VE pattern and the evolution of lesions on serial CT were found to be associated with the time interval from the onset of symptoms to the initial CT scan. Regarding types I and III, the lesions with progression tended to have a significantly shorter time interval than those with absorption (all $P < 0.05$). Type II and IV tended to have a short time interval.

3.6. Comparison of frequencies of the VE pattern in COVID-19 under different lesion sizes and clinical classifications

For the 106 patients with COVID-19, Table 4 summarizes the relationships between frequencies of the VE pattern versus lesion sizes and clinical classification associated with disease severity. Significant differences in the frequencies of the VE pattern were observed between <3-cm lesions and 3–5-cm lesions, 3–5-cm lesions and >5-cm lesions, <3-cm lesions and >5-cm lesions, respectively (all $P < 0.001$), indicating that the larger the lesion, the higher the occurrence of the VE pattern. Compared with those with the common type, patients with the severe–critical type had a significantly higher incidence of the VE pattern ($P < 0.001$).

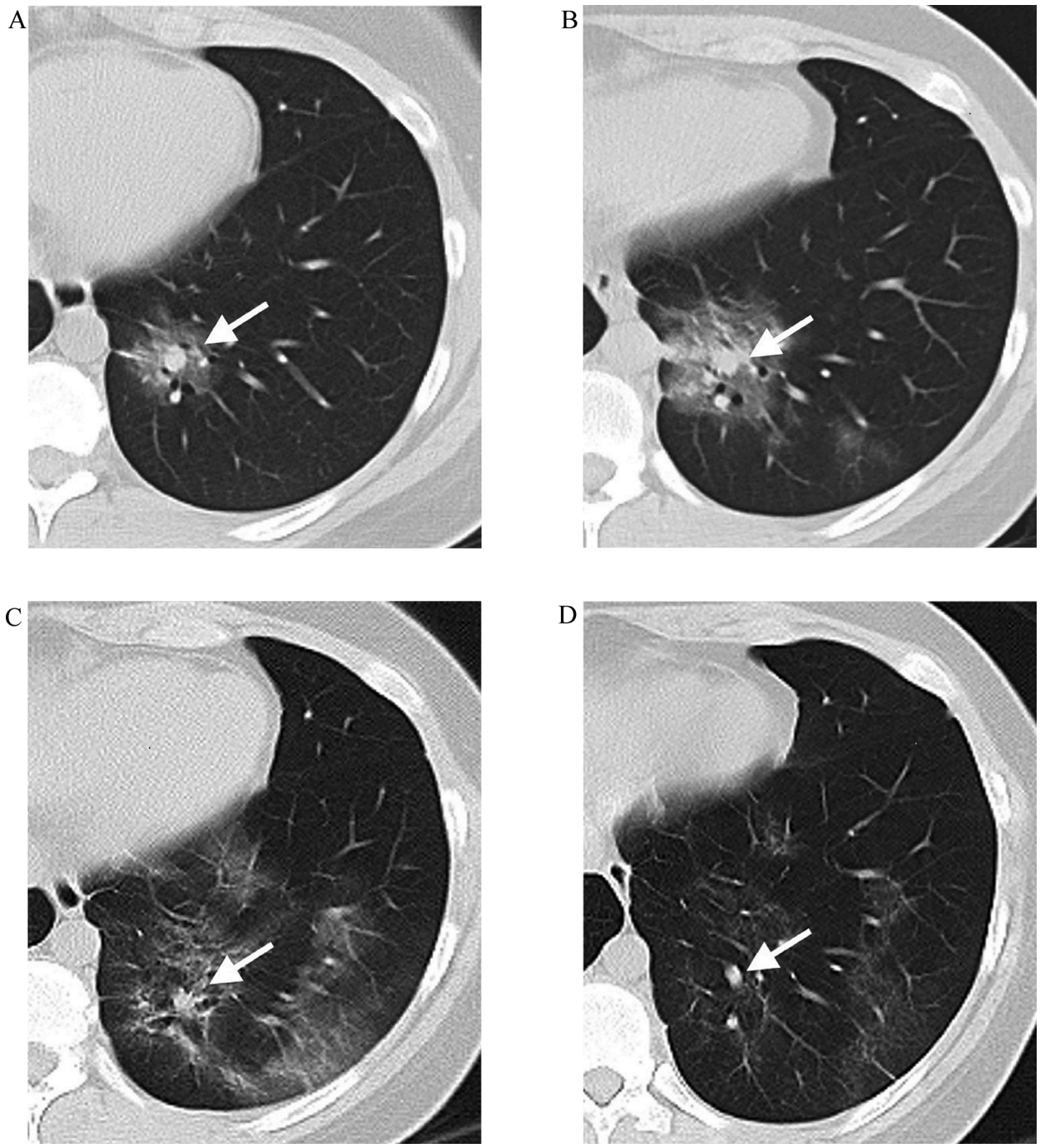

Fig. 1. A 19-year-old female with COVID-19. **A** Initial computed tomography (CT) (1 day from onset) showing a subpleural round GGO in the left lower lobe. Note that a dilated vessel (white arrow) in the center of the lesion similar to a target, resulting in the central vascular sign; **B** Follow-up CT (4 days from onset) showing the lesion is enlarged with internal vessels further dilated (white arrow); **C** Follow-up CT (9 days from onset) showing this lesion is absorbed with internal vessels thinner (white arrow); **D** Follow-up CT (14 days from onset) showing the lesion is further absorbed and internal vessels further thinner (white arrow).

4. Discussion

Recently, some investigators have shown that angiotensin-converting enzyme-2 (ACE-2) may be a functional receptor for SARS-CoV-2 infections and plays a key role in the development and progression of COVID-19 [15,16]. ACE-2 is abundantly present in lung alveolar epithelial cells and vascular endothelial cells and weakly expressed in epithelial cells of bronchial mucosa [17]. Therefore, the lung is the main target. The present study first analyzed general features of COVID-19 based on the initial CT images. The lesions were predominantly peripheral and multilobar. This distribution of COVID-19 may be attributed to the small size of SARS-CoV-2 [18]. After entering the respiratory tract, the virus can directly invade the terminal bronchioles and adjacent acini, resulting in a subpleural distribution. Meanwhile, it can easily disperse in the lung through the alveolar pore and cause multiple lesions. GGO was the most commonly encountered lesion density type. The lower lobe was preferentially affected, followed by the upper lobe; the right middle lobe was the least commonly involved. The lesions exhibited many morphologies and sizes. These findings were consistent with some earlier reports [9–13]. However, several studies have found that aforementioned CT appearances of COVID-19 overlap with those of respiratory tract infections caused by other viruses [12,13], similar to

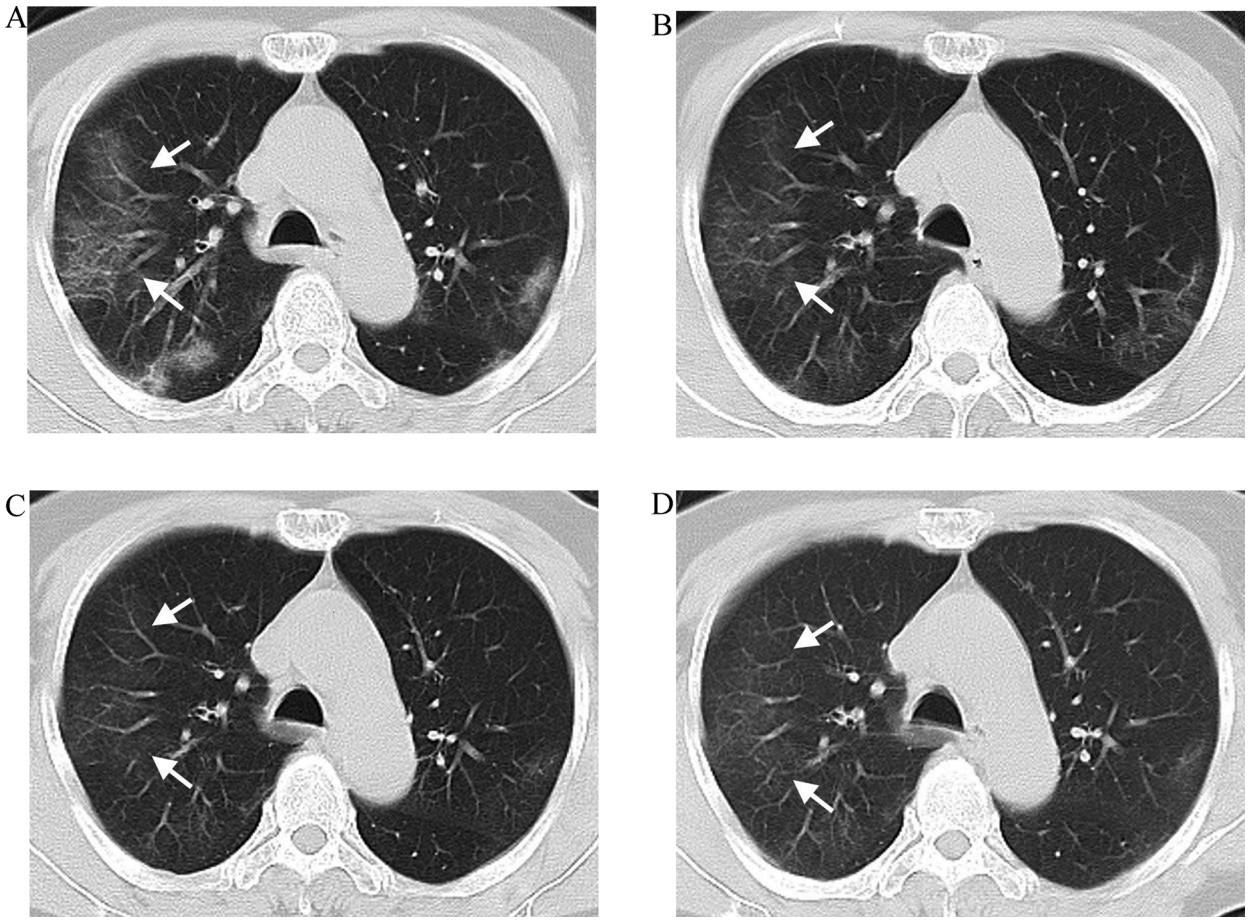

Fig. 2. A 72-year-old female with COVID-19. **A** Initial computed tomography (CT) (13 days from onset) showing a subpleural fan-shaped GGO in the right upper lobe. Note that vessels within the lesion increased and dilated (white arrow) and their trunks extending into the lesion from its tip facing the hilar similar to a ginkgo leaf, resulting in ginkgo leaf sign; **B–D** Follow-up CT (19, 25, and 31 days from onset, respectively) showing the lesion is absorbed gradually and the dilated vessel returns to normal (white arrow).

our results.

In this study, we found that COVID-19 had a significantly higher frequency (83.02 %, 88/106) of the VE pattern than IVP (19.23 %, 10/52), suggesting that the VE pattern is a valuable CT feature for discriminating these two diseases. Zhou et al. [10] analyzed the CT features of 62 patients with COVID-19 pneumonia and found that 45.2 % (28/62) patients showed vascular dilation, which is somewhat lower than that indicated in our study. The reason for this may lie in the differences in the evaluation criteria of the VE pattern and the study sample size. A study by Bai et al. [12] indicated that COVID-19 was more likely to have vascular thickening, which was then thought to be one of the most distinguishing features for COVID-19, than non-COVID-19 pneumonia; this finding is consistent with our results. The VE pattern may be attributed to vascular dilation and damage characterized by endothelial injury and enhanced permeability resulting from a combination of coronavirus-induced direct cytopathic effects and virus-triggered host immune reactions accompanied by massive accumulation of pro-inflammatory factors in the lung [19–21]. For the higher occurrence of the VE pattern in COVID-19, we speculated that pulmonary vessels might be more vulnerable in COVID-19 than in IVP and that the expression pattern of ACE-2 in the lung might explain this [17].

This study identified four types of dynamic changes in the VE pattern on serial CT that were closely associated with the evolution of lesions and time interval from the onset of symptoms to initial CT scan. The results of the present work showed no matter which the VE pattern was present on initial CT, if the vessels further dilated on follow-up CT, the lesions always progressed, which was usually observed soon after illness onset. Most lesions showed resolution in the absence of the VE pattern on all CT scans and were often detected long after the onset of symptoms. These results indicated that disease progression always accompanied aggravation of vascular injury. More serious vascular inflammatory responses showed more obvious increases in vascular diameter and permeability, and more exudation in the alveolar spaces. We found that some lesions with the VE pattern on initial CT but without further vascular dilation on follow-up CT were associated with different outcomes, which were further proved to be related to the time from the onset of symptoms to the initial CT. The improved lesions tended to have a longer interval and vice versa. This can be supported by the results of a previous study which found that 83 % of patients with COVID-19 showed disease progression on CT early after illness onset [22]. If patients undergo a CT scan long after the onset of symptoms, these CT progression-related changes may be missed, and we can only observe these CT performances related to absorption. Hence, the dynamic changes in the VE pattern on follow-up CT combined with the time interval after the onset of symptoms may help predict the evolution of lesions in the short run. Additionally, the VE pattern was found to be more commonly seen in larger lesions and in patients with severe–critical type COVID-19, indicating that vascular changes in COVID-19 were closely related to lesion size and pneumonia severity.

This study has several limitations. First, given the large number of small vessels within or around the lesions we studied, it was difficult to determine whether the VE pattern was present by measuring the diameter of each vessel and calculating the average value. Therefore, we lack an objective quantitative index to confirm the presence of the VE

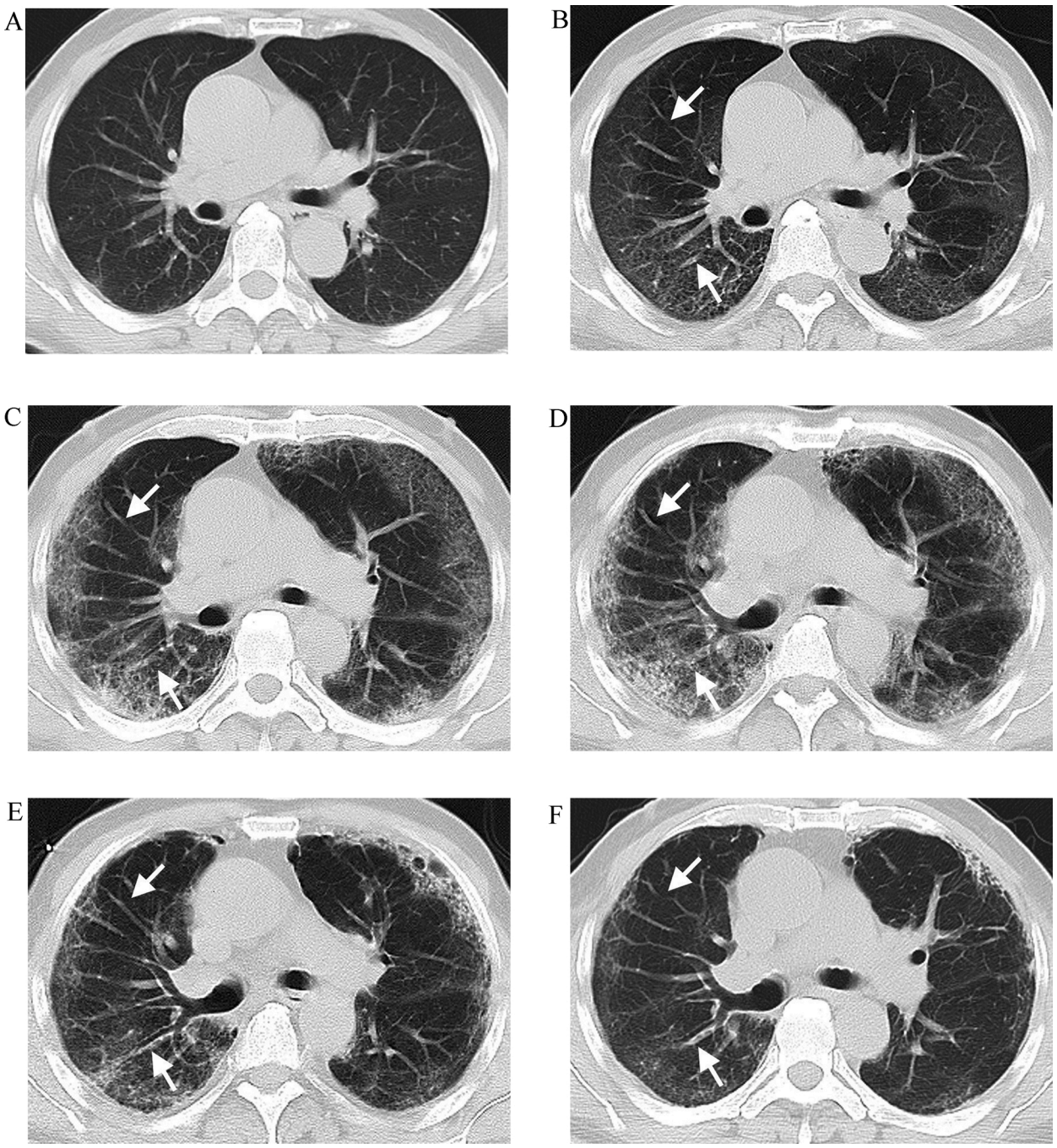

Fig. 3. A 59-year-old male with COVID-19. **A** Initial computed tomography (CT) (1 day from onset) showing a few patchy GGOs in both lungs in the absence of the VE pattern; **B–D** Follow-up CT (7, 12, and 17 days from onset, respectively) showing the lesion progresses with the VE pattern. Note that multiple nearly parallel and dilated vessels vertically entering into subpleural arch-shaped lesions similar to a comb, resulting in the comb sign (white arrow); **E–F** Follow-up CT (24 and 31 days from onset, respectively) showing the lesions are absorbed gradually and the dilated vessels become thin (white arrow).

pattern. Second, our study sample size was small. Third, considering that no patients underwent contrast-enhanced scanning in this study, we did not address the origin of enlarged vessels. Future studies with larger sample sizes are needed for a more comprehensive analysis and to substantiate our findings.

In conclusion, the VE pattern is a useful CT sign for differentiating COVID-19 from IVP, which correlates with more extensive or serious disease. A good understanding of the CT characteristics of the VE pattern may contribute to the early and accurate diagnosis of COVID-19 and prediction of the evolution of lesions.

CRediT authorship contribution statement

Qi Li: Conceptualization, Methodology, Writing - original draft. **Xing-Tao Huang:** Methodology, Formal analysis, Writing - original draft. **Chun-Hua Li:** Investigation, Project administration. **Dan Liu:** Investigation, Project administration. **Fa-Jin Lv:** Conceptualization, Writing - review & editing, Supervision.

Declaration of Competing Interest

None declared.

Table 3
Dynamic changes of the vascular enlargement pattern in coronavirus disease 2019 on serial computed tomography and their relationships with the evolution of lesions and time interval from onset to initial computed tomography.

Categories	VE pattern on initial CT	VE pattern on follow-up CT	Evolution of lesions	Number of lesions	Time interval from onset to initial CT	*P* value
Type I	absence	absence	improvement	115	10.00 ± 7.00	0.005[a]
			progression → improvement	15	3.00 ± 6.00	
Type II	absence	presence → becoming thin or unchanged	improvement	0	–	–
			progression → improvement	30	3.50 ± 4.00	
Type III	presence	becoming thin or unchanged	improvement	90	9.00 ± 4.00	0.021[a]
			progression → improvement	146	7.00 ± 6.00	
Type IV	presence	further enlarged → becoming thin or unchanged	improvement	0	–	–
			progression → improvement	134	2.00 ± 4.25	

VE, vascular enlargement; CT, computed tomography.
[a] Mann–Whitney *U* test; Time interval from onset to initial CT is expressed as median ± interquartile range (days).

Table 4
Comparison of frequencies of the vascular enlargement pattern in coronavirus disease 2019 under different lesion sizes and clinical classifications.

Characteristics	Frequencies of the VE pattern	*P* value
Lesion sizes		
3 cm	52.00 % (143/275 lesions)	< 0.001[a,d]
3–5 cm	78.50 % (84/107 lesions)	< 0.001[b,d]
>5 cm	96.62 % (143/148 lesions)	< 0.001[c,d]
Clinical classifications		
Common type	74.29 % (52/70 patients)	< 0.001[d]
Severe–critical type	100 % (36/36 patients)	

VE, vascular enlargement.
[a] 3 cm vs. 3–5 cm.
[b] 3–5 cm vs. > 5 cm.
[c] 3 cm vs. > 5 cm.
[d] Chi-squared test.

Acknowledgements

This study was supported by Chongqing Scientific & Technological Support Funds (cstc2017jcyjAX0281) and Chongqing Health and Family Planning Commission Foundation (2017MSXM010) of China.

References

[1] Y.R. Guo, Q.D. Cao, Z.S. Hong, Y.Y. Tan, S.D. Chen, H.J. Jin, et al., The origin, transmission and clinical therapies on coronavirus disease 2019 (COVID-19) outbreak - an update on the status, Mil. Med. Res. 7 (2020) 11, https://doi.org/10.1186/s40779-020-00240-0.
[2] V.M. Corman, O. Landt, M. Kaiser, R. Molenkamp, A. Meijer, D.K. Chu, et al., Detection of 2019 novel coronavirus (2019-nCoV) by real-time RT-PCR, Euro Surveill. 25 (2020) 2000045, https://doi.org/10.2807/1560-7917.ES.2020.25.3.2000045.
[3] CDC 2019-Novel Coronavirus (2019-nCoV) Real-Time RT-PCR Diagnostic Panel; Division of Viral Diseases, U.S. Centers for Disease Control and Prevention, Atlanta, GA, 2020.
[4] X. Xie, Z. Zhong, W. Zhao, C. Zheng, F. Wang, J. Liu, Chest CT for typical coronavirus disease 2019 (COVID-19) pneumonia: relationship to negative RT-PCR testing, Radiology 296 (2020) E41–E45, https://doi.org/10.1148/radiol.2020200343.
[5] Y. Fang, H. Zhang, J. Xie, M. Lin, L. Ying, P. Pang, et al., Sensitivity of chest CT for COVID-19: comparison to RT-PCR, Radiology 296 (2020) E115–E117, https://doi.org/10.1148/radiol.2020200432.
[6] T. Ai, Z. Yang, H. Hou, C. Zhan, C. Chen, W. Lv, et al., Correlation of chest CT and RT-PCR testing in coronavirus disease 2019 (COVID-19) in China: a report of 1014 cases, Radiology 296 (2020) E32–E40, https://doi.org/10.1148/radiol.2020200642.
[7] C. Long, H. Xu, Q. Shen, X. Zhang, B. Fan, C. Wang, et al., Diagnosis of the coronavirus disease (COVID-19): rRT-PCR or CT? Eur. J. Radiol. 126 (2020) 108961, https://doi.org/10.1016/j.ejrad.2020.108961.
[8] P. Huang, T. Liu, L. Huang, H. Liu, M. Lei, W. Xu, et al., Use of chest CT in combination with negative RT-PCR assay for the 2019 novel coronavirus but high clinical suspicion, Radiology 295 (2020) 22–23, https://doi.org/10.1148/radiol.2020200330.
[9] S. Salehi, A. Abedi, S. Balakrishnan, A. Gholamrezanezhad, Coronavirus disease 2019 (COVID-19): a systematic review of imaging findings in 919 patients, AJR Am. J. Roentgenol. 215 (2020) 87–93, https://doi.org/10.2214/AJR.20.23034.
[10] S. Zhou, Y. Wang, T. Zhu, L. Xia, CT features of coronavirus disease 2019 (COVID-19) pneumonia in 62 patients in Wuhan, China, AJR Am. J. Roentgenol. 214 (2020) 1287–1294, https://doi.org/10.2214/AJR.20.22975.
[11] R. Han, L. Huang, H. Jiang, J. Dong, H. Peng, D. Zhang, Early clinical and CT manifestations of coronavirus disease 2019 (COVID-19) pneumonia, AJR Am. J. Roentgenol. 215 (2020) 338–343, https://doi.org/10.2214/AJR.20.22961.
[12] H.X. Bai, B. Hsieh, Z. Xiong, K. Halsey, J.W. Choi, T.M.L. Tran, et al., Performance of radiologists in differentiating COVID-19 from viral pneumonia on chest CT, Radiology 296 (2020) E46–E54, https://doi.org/10.1148/radiol.2020200823.
[13] S.O. Onigbinde, A.S. Ojo, L. Fleary, R. Hage, Chest computed tomography findings in COVID-19 and influenza: a narrative review, Biomed. Res. Int. (2020) 6928368, https://doi.org/10.1155/2020/6928368.
[14] General Office of National Health Committee, Notice on the Issuance of a Program for the Diagnosis and Treatment of Novel Coronavirus (2019-nCoV) Infected Pneumonia, trial revised 5th ed., 2020.
[15] X. Xu, P. Chen, J. Wang, J. Feng, H. Zhou, X. Li, et al., Evolution of the novel coronavirus from the ongoing Wuhan outbreak and modeling of its spike protein for risk of human transmission, Sci. China Life Sci. 63 (2020) 457–460, https://doi.org/10.1007/s11427-020-1637-5.
[16] A.M. South, D.I. Diz, M.C. Chappell, COVID-19, ACE2, and the cardiovascular consequences, Am. J. Physiol. Heart Circ. Physiol. 318 (2020) H1084–H1090, https://doi.org/10.1152/ajpheart.00217.2020.
[17] I. Hamming, W. Timens, M.L. Bulthuis, A.T. Lely, G. Navis, H. van Goor, Tissue distribution of ACE2 protein, the functional receptor for SARS coronavirus. A first step in understanding SARS pathogenesis, J. Pathol. 203 (2004) 631–637, https://doi.org/10.1002/path.1570.
[18] N. Zhu, D. Zhang, W. Wang, X. Li, B. Yang, J. Song, et al., A novel coronavirus from patients with pneumonia in China, 2019, N. Engl. J. Med. 382 (2020) 727–733, https://doi.org/10.1056/NEJMoa2001017.
[19] L.B. Ware, M.A. Matthay, The acute respiratory distress syndrome, N. Engl. J. Med. 342 (2000) 1334–1349, https://doi.org/10.1056/NEJM200005043421806.
[20] Y. Imai, K. Kuba, S. Rao, Y. Huan, F. Guo, B. Guan, et al., Angiotensin-converting enzyme 2 protects from severe acute lung failure, Nature 436 (2005) 112–116, https://doi.org/10.1038/nature03712.
[21] J. Liu, X. Zheng, Q. Tong, W. Li, B. Wang, K. Sutter, et al., Overlapping and discrete aspects of the pathology and pathogenesis of the emerging human pathogenic coronaviruses SARS-CoV, MERS-CoV, and 2019-nCoV, J. Med. Virol. 92 (2020) 491–494, https://doi.org/10.1002/jmv.25709.
[22] Y. Xiong, D. Sun, Y. Liu, Y. Fan, L. Zhao, X. Li, et al., Clinical and high-resolution CT features of the COVID-19 infection: comparison of the initial and follow-up changes, Invest. Radiol. 55 (2020) 332–339, https://doi.org/10.1097/RLI.0000000000000674.